Intramolecular structural parameters are key modulators of the gel-liquid transition in coarse grained simulations of DPPC and DOPC lipid bilayers

Stefan Jaschonek[1], Michele Cascella*[2], Jürgen Gauss[1], Gregor Diezemann[1], and Giuseppe Milano[3]

[1]Institut für Physikalische Chemie, Universität Mainz, Duesbergweg 10-14, D-55128 Mainz, Germany
[2]Department of Chemistry and Hylleraas Centre for Quantum Molecular Sciences, University of Oslo, Postboks 1033 Blindern, N-0315 Oslo, Norway
[3]Dipartimento di Chimica e Biologia, Università di Salerno, Via Giovanni Paolo II 132, I-84084, Fisciano, Italy

January 10, 2019

Abstract

The capability of coarse-grained models based on the MARTINI mapping to reproduce the gel-liquid phase transition in saturated and unsaturated model lipids was investigated. We found that the model is able to reproduce a lower critical temperature for 1,2-dioleoyl-*sn*-glycero-3-phosphocholine (DOPC) with respect to 1,2-dipalmitoyl-*sn*-glycero- 3-phosphocholin (DPPC). Nonetheless, the appearance of a gel phase for DOPC is strictly dependent on the intramolecular parameters chosen to model its molecular structure. In particular, we show that the bending angle at the coarse grained bead corresponding to the unsaturated carbon-carbon bond acts as an order parameter determining the temperature of the phase transition. Structural analysis of the molecular dynamics simulations runs evidences that in the gel phase, the packing of the lipophilic tails of DOPC assume a different conformation than in the liquid phase. In the latter phase, the DOPC geometry resembles that of the relaxed free molecule. DPPC:DOPC mixtures show a single phase transition temperature, indicating that the observation of a phase separation between the two lipids requires the simulation of systems with sizes much larger than the ones used here.

1 Introduction

Biomembranes are soft condensed matter assemblies that are crucial constituents of cells. Apart from their structural role in defining the cell wall and in determining the boundaries of organelles, biomembranes are directly involved in several biochemical processes associated to the cellular metabolism. For example, biomembranes can partition cellular spaces, can create rafts that facilitate the localization of specific protein complexes, or can be directly involved into the highly controlled trafficking and delivery of specific substances. [1, 2, 3] Such complex and differentiated dynamic roles are associated to the ability of biomembranes to change their morphology according to their chemical composition and according to external physical or chemical conditions like temperature [4, 5, 6, 7], ionic strength [8, 9], or lateral tension [10, 11, 12, 13, 14].

The complex chemical composition and the dynamics covering a multitude of time scales hamper a straightforward experimental determination of the structure on a molecular scale. The model on which the modern view of biological membranes is based is the *fluid mosaic* model of Singer and Nicholson [15]. This model describes a biomembrane as a fluid bilayer composed of a mixture of lipids, in which embedded or adhered proteins or molecules are free to move on and into the bilayer plane.

Because of the complexity of biomembrane structures, experiments are usually conducted on simplified model systems, e.g., so-called *reconstituted lipid bilayers*. These systems are composed of only very few lipid species (typically one or two), in which specific proteins or lipophilic substances like sterols are eventually embedded. [2] These model systems show the typical phase behavior of membranes with a high temperature liquid phase (L_α) and a gel phase (L_β) for lower temperatures.[2, 16] However, due to their simple structures they can be rather easily investigated with a variety of techniques. These include spectroscopic methods allowing to study their structure [17, 18, 19] and dynamics[20, 21].

As in many other areas of biological and chemical physics, computer simulations can provide important structural and dynamical information about lipid bilayers at the molecular scale.[2, 22, 23] However, despite the increasing growth of computing power that allows the simulation of larger systems for longer times, simulations based on all-atom models of lipid bilayers are still hampered by severe limitations. These include the relatively limited size of the simulation box, which constrains the characteristic length of the lipid bilayer deformations that can be investigated, the necessity to use periodic boundary conditions that can introduce a finite-size bias on the aggregation states and the diffusion properties, and the relatively short times accessible to the investigation, usually much shorter than those required to observe large-scale events like membrane reorganization.[24]

Coarse-grained (CG) modelling [25, 26, 27, 28, 29] thus offers a valid alternative to all-atom based simulations for the description of lipid bilayers. In CG models the chemical structure of the molecules is represented by so-called *beads* that are formed by merging a given number of neighboring atoms into one unit. The beads act as effective interactions sites during the simulation of the system. Both the choice of the mapping of the molecular moieties onto the beads and the functional form used for the interaction potential intrinsically define the CG model. [30, 31, 32, 33, 34, 35]

Starting with the very early studies using CG representations,[27] up to date, CG simulations capturing important chemical details allowed to investigate large structures and complex mixtures, and to address mechanical deformations and associated effects on both structural and dynamical properties.[36] For example, CG simulations helped to obtain a molecular description for the softening of gel-phase lipid membranes upon bending, and thus to understand the formation and localization of curved areas.[37, 14, 13]

The effective potentials used in CG models have to take into account the loss of structural and chemical information that result from the mapping procedure.[22, 38] Such potentials are typically calibrated on data sets obtained either from experimental measurements or from higher-resolution models. As a result, CG models may be biased toward specific properties or thermodynamic conditions and may lack the universality required to reproduce the behavior of a system within different regions of its phase diagram. [6, 39]

In the present study, we focus on the performance of the MARTINI force-field [25], one of the most popular CG potentials used today for the description of the liquid-gel transition in bilayers constituted by simple models of saturated and mono-unsaturated lipids. We find that, while the transition is well reproduced qualitatively in saturated moieties, the liquid-gel phase change in mono-unsaturated lipids strongly depends on the geometrical representation of the fatty tails. In particular, our data show that the bending angle at the unsaturated moiety is a key parameter that determines both the existence and the location of the transition as a function of temperature.

2 Computational methods

System setup. We used 1,2-dipalmitoyl-*sn*-glycero- 3-phosphocholin (DPPC) and 1,2-dioleoyl-*sn*-glycero-3-phosphocholine (DOPC) as models for saturated and unsaturated lipids. All molecules were represented using standard MARTINI coarse-grained parameters [25]. The bonded parameters of these models are illustrated in Figure 1. The simulations were performed using the GROMACS 4.6 program package.[40] For the short-range inter-

actions a cut-off of 0.9 nm was used. The long-range Coulomb interactions and the van der Waals interactions were treated using shifted potentials.[41, 42] The used simulation time step was 40 fs which is possible because the bonded interactions were constrained to their equilibrium values using the LINCS-algorithm [43]. The neighbor list was updated every 400 fs. The system was coupled to a Berendsen thermostat[44] (temperature coupling parameter $\tau_T = 4$ ps) and to a Berendsen barostat[44] (pressure coupling parameter $\tau_p = 4$ ps and reference pressure $p_0 = 1$ bar).

We investigated three independent lipid systems at two different sizes (small and large). One contains only DPPC, one only DOPC, and the third one contains a 1:1 mixture of DPPC:DOPC. The smaller system consists of 128 lipids and the larger one of 1152 lipids. The simulation boxes were set up according to the following protocol. First, the simulated lipids were randomly distributed in the simulation box (8 nm × 8 nm × 8 nm or 24 nm × 24 nm × 8 nm) and the energy of the system was minimized. Then, water and the anti-freeze particles [25] were added and the energy was again minimized. After that, a NVT simulation was performed until a regular bilayer was formed. Finally, a NPT simulation using a semi-isotropic pressure coupling was run to equilibrate the system. This equilibration run was stopped when both the pressure and the temperature reached the desired value. The box sizes for the different systems at 323 K are 6.32 nm × 6.32 nm × 10.19 nm (system containing 128 DPPC), 6.65 nm × 6.65 nm × 9.88 nm (system containing 128 DOPC), and 6.39 nm×6.39 nm×11.36 nm (system containing 64 DPPC and 64 DOPC). The box size for the large systems is approximately 19.2 nm × 19.2 nm × 11.4 nm

The phase transition from the liquid-crystalline phase L_α to the gel phase L_β was investigated by starting from the well equilibrated systems at 323 K. The systems were cooled down to a lower temperature and after equilibration for $\approx$ 200 ns (small system) or $\approx$ 500 ns (large system) the properties of interest were measured over $\approx$ 200 ns (small system) or $\approx$ 500 ns (large system) and averaged.

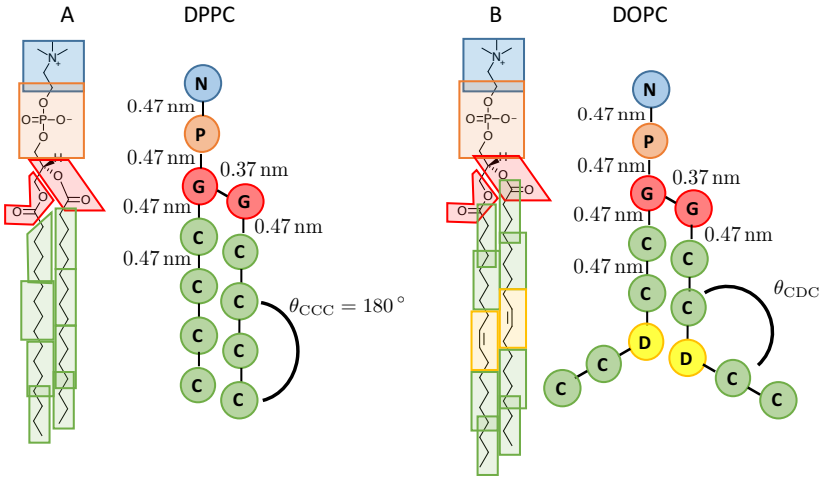

θ_{CDC} / °	T_{trans} / K
132.5	250
138.0	270
145.0	280

K_{CDC}/kJ/mol	$T_{\mathrm{trans}}^{\mathrm{DOPC}}$ / K
25	260
40	252.5
45	250
50	252.5
60	252.5
90	250

Figure 1: Sketch illustrating the structure, mapping, and parameters of the MARTINI models of DPPC (**A**) and DOPC (**B**). **C:** Adjusted parameters and resulting transition temperatures T_{trans}. Upper panel: different tested equilibrium angles θ_{CDC}. Lower panel: Different tested K_{CDC} for $\theta_{\mathrm{CDC}} = 132.5\,^\circ$.

3 Results and discussion

One-component DPPC system. The DPPC MARTINI model is known to reproduce the liquid-gel transition from the fluid or liquid-crystalline phase L_α to the gel phase L_β at a temperature of $T_{\text{trans}} = 295 \pm 5\,\text{K}$, and this has already extensively been described in [45]. The obtained transition temperature is in semi-quantitative agreement with the experimental data for DPPC of $T_{\text{trans}}^{\text{exp}} = 314\,\text{K}$. [16] While the simulations presented in [45] provided detailed information about the dynamics of the liquid-to-gel transition, our focus is on the temperature dependence of the order parameter and other important variables. The use of two different DPPC bilayer systems (a small patch consisting of 128 lipids and large one with 11552 lipids) allowed us to rule out system-size effects [46, 47] and to validate the use of the smaller system. To induce a phase transition a well equilibrated system was cooled down to a lower temperature from a starting temperature of $T = 323\,\text{K}$. The phase L_β differs from the phase L_α by the following points: (i) the lipid tails are almost fully extended with a few gauche defects remaining and (ii) the area per lipid (APL) is smaller than in the liquid phase.

The conformational transition from a more disordered to an ordered orientation of the lipid tails was characterized by a change in the order parameter $\langle P_2 \rangle = \frac{1}{2}\langle 3\cos^2\varphi - 1\rangle$ where φ is the angle between the long molecular axis (cf. inlay Figure 2 **A**) and the normal vector to the bilayer plane. A value of $\langle P_2 \rangle = 1$ points to the existence of a perfect alignment of the lipid tail with the bilayer normal vector, a value $\langle P_2 \rangle = 0$ corresponds instead to a random orientation.

Figure 2 **A** reports the order parameter $\langle P_2 \rangle$ as a function of temperature for the two systems of different sizes. The transition is manifested by a sharp change of $\Delta \langle P_2 \rangle \approx 0.17$ (see figure 2 **A**). The obtained values for the large system (red symbols) and the small system (black symbols) are in quantitative agreement in the regions of stability of both phases. The smaller system predicts the liquid to gel transition at a slightly lower temperature (290 K) than what is observed for the larger system (293 K). This discrepancy lies within the uncertainty reported in the original study[45]; therefore, we conclude that the small system captures the relevant physics of the transition.

Together with the $\langle P_2 \rangle$ parameter, we determined the angle $\bar{\theta}_{\text{CCC}}$ (see Figure 1) at different temperatures. In the L_α-phase we found $\bar{\theta}_{\text{CCC}} \approx 160\,^\circ$ and in the L_β-phase $\bar{\theta}_{\text{CCC}} \approx 145\,^\circ$. This indicates that the local packing of the lipid tails affects their molecular structure, i.e., the averaged structure is the result of a compromise between the tendency to increase intermolecular contacts and the cost for the deformation of the intramolecular geometry induced by that. In the liquid L_α-phase, the reduced intermolecular packing

allows a relaxation of the molecular structure to values closer to the equilibrium structure of the individual molecule.

The lateral box length at $T = 240\,\mathrm{K}$ (L_β-phase) is 86% of the width in the L_α-phase. From the knowledge of the box lengths the area per lipid (APL) can be calculated as $\mathrm{APL} = \frac{d_x d_y}{N_{\mathrm{lipid}}/2}$ where d_x and d_y are the lateral box lengths and N_{lipid} is the number of lipids. Figure 2 **A** shows the area per lipid as a function of the temperature. As expected, we observed a sudden decrease in the APL at the transition temperature $T = 290\,\mathrm{K}$. This sudden decrease of roughly $0.8\,\mathrm{nm}^2$ is consistent with the closer packing of the lipid chains expected in the gel phase L_β (cf. Figure 2 **B** and **C**).

Apart from the structural parameters just discussed, we determined the lateral diffusion coefficients D_{xy} in both phases and find a decrease of about two orders of magnitude in the gel phase (L_α: $D_{xy} \approx 10^{-7}\,\mathrm{cm}^2/\mathrm{s}$ and L_β: $D_{xy} \approx 10^{-9}\,\mathrm{cm}^2/\mathrm{s}$, independent of system size). We attribute this decreased mobility to the rigid structure in the L_β-phase.

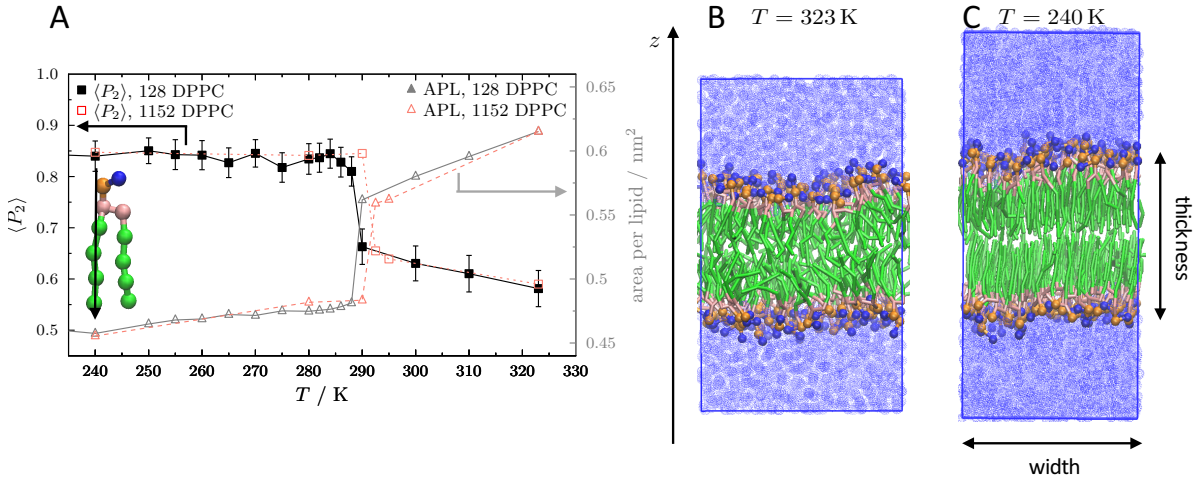

Figure 2: **A:** Order parameter $\langle P_2 \rangle$ (black squares) and APL (grey squares) vs temperature for DPPC. The red symbols show the values for the larger system. The inlay shows a single DPPC as a stick model. The arrow indicates the long molecular axis. **B** and **C**: Snapshots of the bilayer at two different temperatures. **B** is showing the system in the L_α-phase at $T = 323\,\mathrm{K}$ and **C** the L_β-phase at $T = 240\,\mathrm{K}$.

One-component DOPC system. As already noted in the introduction, the original MARTINI model of DOPC does not predict a liquid-to-gel transition in the relevant temperature range of $T \geq 240\,\mathrm{K}$. Recently, a modified DOPC model characterized by an equilibrium value of $145\,^\circ$ for θ_{CDC} was introduced.[48] This value was obtained as the result of a different mapping procedure. In the present work, we repeated the study on the liquid-to-gel transition for DOPC models with different values for the same angle, ranging from the original $\theta_{\mathrm{CDC}} = 120\,^\circ$ value [25] to $\theta_{\mathrm{CDC}} = 145\,^\circ$ [25]. In Figure 3 **A** $\langle P_2 \rangle$, APL and $\bar{\theta}_{\mathrm{CDC}}$ are shown as a function of the temperature. A clear discontinuity for the properties monitored is observed for the models with $\theta_{\mathrm{CDC}} = 132.5\,^\circ$ (**C**), $\theta_{\mathrm{CDC}} = 138\,^\circ$ (**D**) and $\theta_{\mathrm{CDC}} = 145\,^\circ$ (**E**). The obtained transition temperatures T_{trans} are displayed in Figure 1 **C**. T_{trans} ranges from 250 K to 280 K and is increasing with increasing θ_{CDC}-value. In the ordered phase L_β the measured angles $\bar{\theta}_{\mathrm{CDC}}$ are roughly $145\,^\circ$ (**C**), $155\,^\circ$ (**D**) and $160\,^\circ$ (**E**). For **D** and **E** the measured angle $\bar{\theta}_{\mathrm{CDC}}$ is similar to the $\bar{\theta}_{\mathrm{CCC}}$-angle in the gel phase of the DPPC MARTINI model (cf. Figure 2). The DOPC model with an equilibrium angle $\theta_{\mathrm{CDC}} = 132.5\,^\circ$ is able to reproduce the liquid-to-gel transition and additionally models the kink in the gel phase in a chemical meaningful way.

Besides altering the equilibrium angle θ_{CDC} also the corresponding force constant K_{CDC} ($[K_{\mathrm{CDC}}] = {}^{\mathrm{kJ}}/_{\mathrm{mol}}$ due to the cosine based angle potential) was changed. For $\theta_{\mathrm{CDC}} = 132.5\,^\circ$ different values for K_{CDC} ranging from $25\,{}^{\mathrm{kJ}}/_{\mathrm{mol}}$ to $90\,{}^{\mathrm{kJ}}/_{\mathrm{mol}}$ were tested with $K_{\mathrm{CDC}} = 45\,{}^{\mathrm{kJ}}/_{\mathrm{mol}}$ being the standard MARTINI value. The tested K_{CDC}-values and the resulting transition temperatures are displayed in Figure 1 **C** (lower panel). Except for the lowest value of $K_{\mathrm{CDC}} = 25\,{}^{\mathrm{kJ}}/_{\mathrm{mol}}$, a variation of K_{CDC} in the range from $40\,{}^{\mathrm{kJ}}/_{\mathrm{mol}}$ to $90\,{}^{\mathrm{kJ}}/_{\mathrm{mol}}$ does not change the transition temperature. Even though the order parameter in the L_β-phase is not changing significantly, the structure of the different DOPC models still depends on the chosen value for K_{CDC}. For temperatures $T < T_{\mathrm{trans}}$, the measured mean angle $\bar{\theta}_{\mathrm{CDC}}$ for $K_{\mathrm{CDC}} \leq 45\,{}^{\mathrm{kJ}}/_{\mathrm{mol}}$ can be larger than $\bar{\theta}_{\mathrm{CDC}} = 137\,^\circ$ which is the angle found at the transition temperature for all tested K_{CDC}-values. The $\bar{\theta}_{\mathrm{CDC}}$ angles for $K_{\mathrm{CDC}} \geq 50\,{}^{\mathrm{kJ}}/_{\mathrm{mol}}$ are smaller than $137\,^\circ$ for temperatures $T < T_{\mathrm{trans}}$. From these observations we conclude that the lipid chains for K_{CDC}-values larger than $50\,{}^{\mathrm{kJ}}/_{\mathrm{mol}}$ in the L_β-phase are bent more than the ones with K_{CDC}-values smaller than $45\,{}^{\mathrm{kJ}}/_{\mathrm{mol}}$.

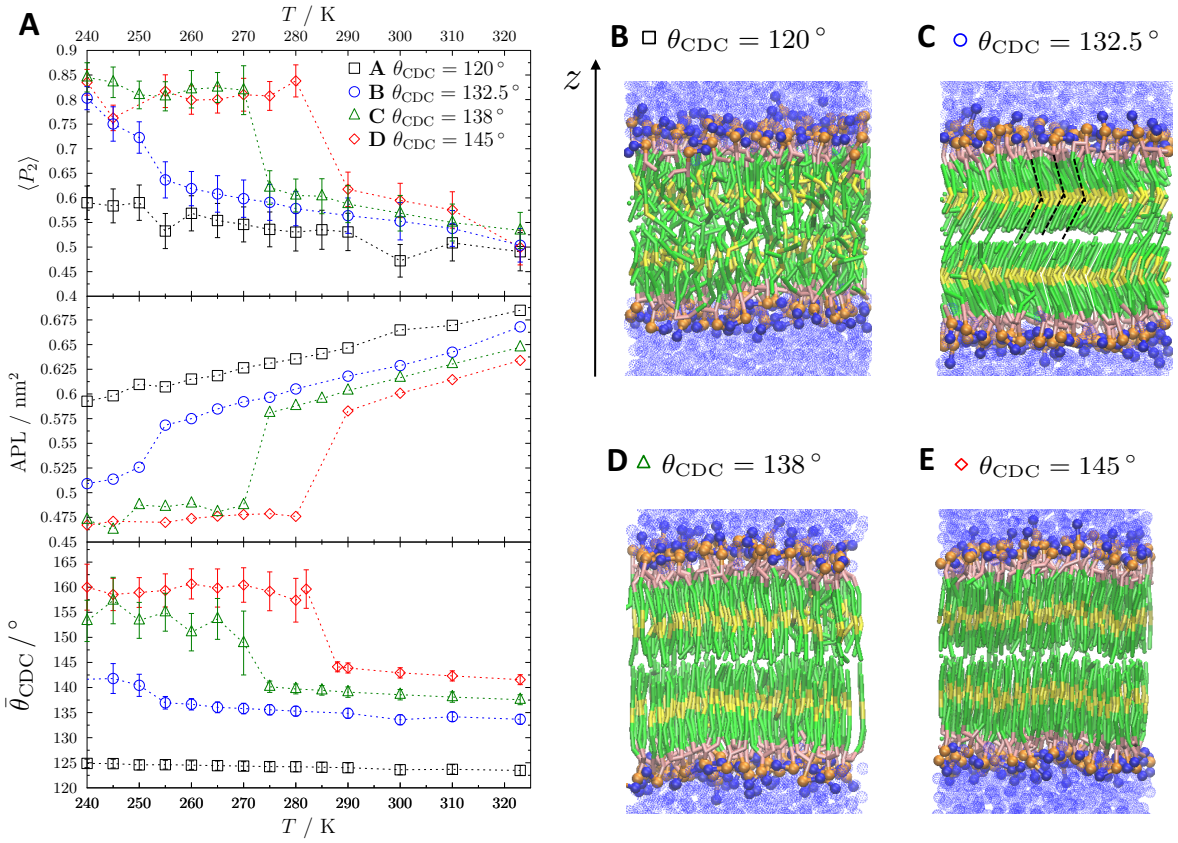

Figure 3: Left panel, **A**: $\langle P_2 \rangle$, APL and measured angle $\bar{\theta}_{\mathrm{CDC}}$ as function of the temperature for different equilibrium θ_{CDC}-angles. Right panel: Snapshots of the DOPC bilayer patches at $T = 240\,\mathrm{K}$ for different DOPC models. **B:** Standard MARTINI model for DOPC [25], $\theta_{\mathrm{CDC}} = 120\,^\circ$, **C:** $\theta_{\mathrm{CDC}} = 132.5\,^\circ$, the dotted lines illustrate the observed kink, **D:** $\theta_{\mathrm{CDC}} = 138\,^\circ$, **E:** $\theta_{\mathrm{CDC}} = 145.5\,^\circ$ as used in [48]. The force constant for all shown angles is $K_{\mathrm{CDC}} = 45\,{}^{\mathrm{kJ}}/_{\mathrm{mol}}$.

Two-component system DPPC/DOPC mixture. In order to test the general applicability of the one-component models DPPC and DOPC, we investigated the phase behavior of the two-component DPPC:DOPC mixture in a 1:1 stoichiometric ratio. Two simulation boxes consisting of 64 DPPC and 64 DOPC and one of 576 DOPC and 576 DPPC were used for the simulations. Here, the DOPC model with an equilibrium angle of $\theta_{\mathrm{CDC}} = 132.5\,^{\circ}$ and a force constant of $K_{\mathrm{CDC}} = 45\,{}^{\mathrm{kJ}}/_{\mathrm{mol}}$ was used. Like for the previously discussed one-component systems of DPPC and DOPC, the results obtained for the large system consisting of 1152 lipids agree with the results for the smaller system with 128 lipids. Therefore, only the smaller system will be discussed in the following.

The left panel of Figure 4 (**A**) compares the properties $\langle P_2 \rangle$, APL, and $\bar{\theta}_{\mathrm{CXC}}$ (X = C, D) plotted as a function of temperature, for the one-component systems and the two-component mixture. The single discontinuity for the order parameter $\langle P_2 \rangle$ and the measured angle $\bar{\theta}_{\mathrm{CXC}}$ in the $270-280\,\mathrm{K}$ temperature range marks the phase transition in the 1:1 DOPC:DPPC two-component system. This temperature is roughly at the midpoint of the transition temperatures of the pure DPPC and DOPC systems. The same discontinuity is seen for the APL, and is also consistent with the behavior of the measured mean angles $\bar{\theta}_{\mathrm{CXC}}$ shown in the lower graph (Figure 4 **A**). In particular, DOPC exhibit a larger value for $\bar{\theta}_{\mathrm{CDC}}$ in the mixture than in the pure system. In the L_{β} phase no tilt is visible and the lipid chains of DOPC seem to be perfectly stretched. This allows a denser packing of the lipid tails and therefore leads to a reduced value of the APL.

The individual DPPC and DOPC components forming the mixture exhibit the gel-liquid transition at the same temperature, indicating that our model system is not undergoing a phase separation. [49] By looking at the bilayer surface in the L_{β}-phase (Figure 4 **D**) and L_{α}-phase (Figure 4 **E**), it is possible to observe that DOPC and DPPC start building some patches, but there is still a significant degree of mixing between the two types of lipids. This observation can be quantified by estimating the average number of neighboring lipids of the same kind residing in the proximity of a lipid. For this type of analysis for each DPPC the number of neighboring DPPC was counted and averaged. Neighboring lipids were determined via a distance criterion r_{neigh} defined via the radial distribution function. The distance criterion r_{neigh} itself is the position of the first minimum in the radial distribution function between the P-beads of the same lipid. r_{neigh} was determined at the temperatures ($240\,\mathrm{K}$ and $323\,\mathrm{K}$) for the DPPC/DOPC system and the one-component systems. For the small and the large variation of the mixed system, there are on average the same amount of DOPC and DPPC lipids within the neighboring distance at both investigated temperatures. This means that a for a small finite-sized

simulation box most of the lipids are at the DPPC/DOPC interface. This is exactly what one would expect for a well-mixed two-component system. In this way we conclude that there is no phase separation for the small system as well as the large system.

This discrepancy from the experimental data indicates a finite size bias present in the simulated systems. In fact, although a small degree of separation is observed, both the small and large simulation boxes are characterized by substantial mixing between the two phases. As a consequence, the sequestration of a sufficiently high number of lipids into single-component patches does not occur.

Finally, we studied the impact of the force constant K_{CDC} on the transition temperature of the mixture. As before, values for K_{CDC} ranging between $25\,{}^{\mathrm{kJ}}/_{\mathrm{mol}}$ and $90\,{}^{\mathrm{kJ}}/_{\mathrm{mol}}$ were investigated and the resulting transition temperatures are listed in Table 1. It is evident that the observed transition temperature is more or less constant and is about 10 K higher than the corresponding temperature in the neat DOPC system (see Figure 1 **C**).

Table 1: Angle CDC $\theta_{\mathrm{CDC}} = 132.5\,^{\circ}$ at different K_{CDC} and their transition temperatures for a mixed DPPC/DOPC system.

$K_{\mathrm{CDC}}/{}^{\mathrm{kJ}}/_{\mathrm{mol}}$	$T_{\mathrm{trans}}^{\mathrm{DPPC/DOPC}}$ / K
25	270
40	265
45	270
50	265
60	270
90	270

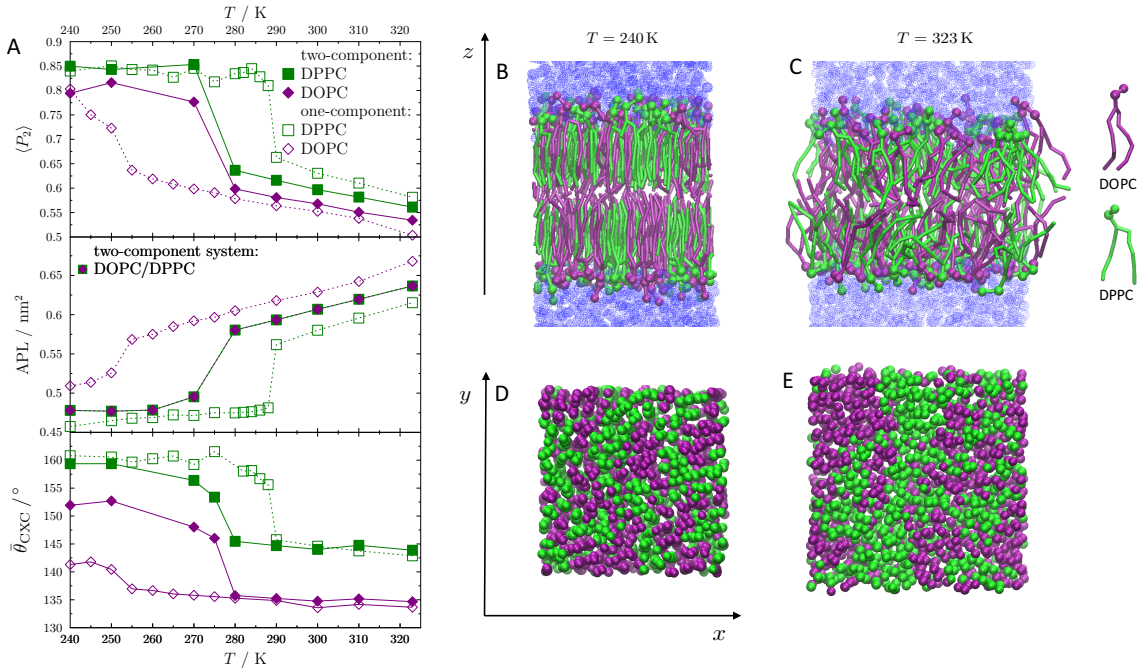

Figure 4: Left panel, **A**: $\langle P_2 \rangle$, APL and $\bar{\theta}_{\mathrm{CXC}}$ as function of the temperature for the two-component DPPC/DOPC system and the one-component DPPC and DOPC systems. For the measured angle $\bar{\theta}_{\mathrm{CXC}}$ (X = C, D) the color coding is as follows: $\bar{\theta}_{\mathrm{CCC}}$ for DPPC is shown in green and $\bar{\theta}_{\mathrm{CDC}}$ is shown in purple. The open symbols represent the one-component system and the full symbols the two-component system. Right panel: Snapshots of two-component DPPC/DOPC at different temperatures (323 K and 240 K) and different perspectives. **B** and **C**: side view of the bilayer patch. **D** and **E**: bilayer surface.

4 Conclusion

In the present work we performed studies on different lipid models based on the MARTINI models for DPPC and DOPC with respect to the description they provide for the liquid-gel transition and the phase separation of a DPPC:DOPC mixture. These phospholipids are the standard examples for a saturated (DPPC) and an unsaturated (DOPC) lipid. The already well studied DPPC MARTINI model [45] was used to introduce the simulation techniques and the differences between the gel phase L_β and the liquid crystalline phase L_α. The properties of DOPC were studied as a function of various model parameters, with a particular focus on the CDC equilibrium angle θ_{CDC} and its associated force constant K_{CDC}. For increasing values of θ_{CDC} the phase transition temperature T_{trans} increases. A value of $\theta_{\mathrm{CDC}} = 132.5\,^\circ$ gives semi-quantitative agreement with the experimental transition temperature whereas the original MARTINI model of DOPC fails to describe the liquid-to-gel transition at all. The phase transition temperature shows little or no dependence on the force constant K_{CDC} in the interval studied ($25 - 90\,\mathrm{kJ/mol}$). On the contrary, K_{CDC} has a marked effect on the structural properties of DOPC in the gel phase and therefore on the observed kink in the lipid tail. For values $K_{\mathrm{CDC}} \geq 50\,\mathrm{kJ/mol}$ the lipid tails are more bent than for $K_{\mathrm{CDC}} \leq 45\,\mathrm{kJ/mol}$.

Furthermore, the liquid-gel transition and the phase separation in DPPC:DOPC mixtures were examined. It is found that the presence of DPPC has a strong impact on DOPC in the gel phase L_β, as if the DOPC lipid chains are now significantly more stretched. This leads to a denser packing of the lipid chains and in a smaller APL and is accompanied with an increase in the order parameter $\langle P_2 \rangle$. The influence of DPPC on DOPC in the liquid phase is still existent but not as strong as in the gel phase. A variation of the force constant K_{CDC} does not result in a change of the transition temperature nor in the structure of the lipid tails. While mixtures of different lipids with significantly different T_{trans} are known experimentally to undergo phase separation, this could not be observed for the systems studied here, indicating that a critical number of lipids, much larger than the ones used here, is necessary to study such aggregation phenomena.

Acknowledgements

Financial support by the Deutsche Forschungsgemeinschaft via the TRR 146 is acknowledged. Further support by the Centre for Theoretical and Computational Chemistry (CTCC), Norwegian Centre of Excellence (CoE).

References

[1] G. van Meer, D. R. Voelker, and G. W. Feigenson, Nat. Rev. Mol. Cell Biol. **9**, 112 (2008).

[2] M. Venturoli, M. Maddalena Sperotto, M. Kranenburg, and B. Smit, Phys. Rep. **437**, 1 (2006).

[3] R. Phillips, J. Kondev, and J. Theriot, Physical biology of the cell, New York, 2009.

[4] D. Papahadjopoulos, K. Jacobson, S. Nir, and I. Isac, Biochim. Biophys. Acta **311**, 330 (1973).

[5] N. Kuerka, S. Tristram-Nagle, and J. F. Nagle, J. Membr. Biol. **208**, 193 (2006).

[6] M. Kranenburg and B. Smit, J. Phys. Chem. B **109**, 6553 (2005).

[7] E. Z. Drobnis et al., J. Exp. Zool. **265**, 432 (1993).

[8] K. L. Jones and C. R. OMelia, J. Membr. Sci. **165**, 31 (2000).

[9] H. Truble and H. Eibl, Proc. Natl. Acad. Sci. U.S.A. **71**, 214 (1974).

[10] M. M. Kozlov and L. V. Chernomordik, Curr. Opin. Struct. Biol. **33**, 61 (2015).

[11] K. Keren, Proc. Natl. Acad. Sci. U.S.A. **108**, 14379 (2011).

[12] J. H. Kim et al., Dev. Cell **32**, 561 (2015).

[13] M. Hu, P. Diggins, and M. Deserno, J. Chem. Phys. **138**, 214110 (2013).

[14] X. Wang and M. Deserno, J. Phys. Chem. B **120**, 6061 (2016).

[15] S. J. Singer and G. L. Nicolson, Science **175**, 720 (1972).

[16] R. Koynova and M. Caffrey, Biochim. Biophys. Acta **1376**, 91 (1998).

[17] C. Dietrich et al., Biophys. J. **80**, 1417 (2001).

[18] A. V. Samsonov, I. Mihalyov, and F. S. Cohen, Biophys. J. **81**, 1486 (2001).

[19] N. Kučerka et al., Biophys. J. **95**, 2356 (2008).

[20] J. Korlach, P. Schwille, W. W. Webb, and G. W. Feigenson, Proc. Natl. Acad. Sci. U.S.A. **96**, 8461 (1999).

[21] S. Nandi et al., Biophys. J. **110**, 2016 (2016).

[22] M. L. Klein and W. Shinoda, Science **321**, 798 (2008).

[23] G. Milano, T. Kawakatsu, and A. De Nicola, Phys. Biol. **10**, 045007 (2013).

[24] T. A. Soares, S. Vanni, G. Milano, and M. Cascella, J. Phys. Chem. Lett. **8**, 3586 (2017).

[25] S. J. Marrink, H. J. Risselada, S. Yefimov, D. P. Tieleman, and A. H. de Vries, J. Phys. Chem. B **111**, 7812 (2007).

[26] W. Shinoda, R. DeVane, and M. L. Klein, J. Phys. Chem. B **114**, 6836 (2010).

[27] M. Orsi and J. W. Essex, PLOS ONE **6**, e28637 (2011).

[28] M. Deserno, K. Kremer, H. Paulsen, C. Peter, and F. Schmid, Computational Studies of Biomembrane Systems: Theoretical Considerations, Simulation Models, and Applications, in From Single Molecules to Nanoscopically Structured Materials, Advances in Polymer Science, pages 237–283, Springer, Cham, 2013, DOI: 10.1007/12_2013_258.

[29] M. Müller, K. Katsov, and M. Schick, Phys. Rep. **434**, 113 (2006).

[30] J. C. Shelley, M. Y. Shelley, R. C. Reeder, S. Bandyopadhyay, and M. L. Klein, J. Phys. Chem. B **105**, 4464 (2001).

[31] J. C. Shelley et al., J. Phys. Chem. B **105**, 9785 (2001).

[32] L. Saiz and M. L. Klein, Acc. Chem. Res. **35**, 482 (2002).

[33] S. J. Marrink, A. H. de Vries, and A. E. Mark, J. Phys. Chem. B **108**, 750 (2004).

[34] G. Brannigan, L. C.-L. Lin, and F. L. H. Brown, Eur. Biophys. J. **35**, 104 (2006).

[35] Q. Shi, S. Izvekov, and G. A. Voth, J. Phys. Chem. B **110**, 15045 (2006).

[36] S. J. Marrink and A. E. Mark, J. Am. Chem. Soc. **125**, 11144 (2003).

[37] H. J. Risselada and S. J. Marrink, Phys. Chem. Chem. Phys. **11**, 2056 (2009).

[38] M. Cascella and S. Vanni, Toward accurate coarse-graining approaches for protein and membrane simulations, in Chemical Modelling, pages 1–52, 2015, DOI: 10.1039/9781782622703-00001.

[39] M. J. Stevens, The Journal of Chemical Physics **121**, 11942 (2004).

[40] B. Hess, C. Kutzner, D. van der Spoel, and E. Lindahl, J. Chem. Theory Comput. **4**, 435 (2008).

[41] T. Darden, D. York, and L. Pedersen, J. Chem. Phys. **98**, 10089 (1993).

[42] M. Allen and D. Tildesley, Computer Simulations of Liquids, Oxford Science Publications, Oxford, 1987.

[43] B. Hess, H. Bekker, H. J. C. Berendsen, and J. G. E. M. Fraaije, J. Comput. Chem. **18**, 1463 (1997).

[44] H. J. C. Berendsen et al., J. Chem. Phys. **81**, 3684 (1984).

[45] S. J. Marrink, J. Risselada, and A. E. Mark, Chem. Phys. Lipids **135**, 223 (2005).

[46] F. Castro-Romn, R. W. Benz, S. H. White, and D. J. Tobias, J. Phys. Chem. B **110**, 24157 (2006).

[47] S. J. Marrink and A. E. Mark, J. Phys. Chem. B **105**, 6122 (2001).

[48] M. D. Daily, B. N. Olsen, P. H. Schlesinger, D. S. Ory, and N. A. Baker, J. Chem. Theory Comput. **10**, 2137 (2014).

[49] T. T. Mills, J. Huang, G. W. Feigenson, and J. F. Nagle, Gen. Physiol. Biophys. **28**, 126 (2009).